Journal of Membrane Science 620 (2021) 118411

Contents lists available at ScienceDirect

Journal of Membrane Science

journal homepage: http://www.elsevier.com/locate/memsci

Modeling and validation of concentration dependence of ion exchange membrane permselectivity: Significance of convection and Manning's counter-ion condensation theory

R.S. Kingsbury, O. Coronell *

Department of Environmental Sciences and Engineering, Gillings School of Global Public Health, The University of North Carolina at Chapel Hill, Chapel Hill, NC, 27599, USA

ARTICLE INFO

Keywords:
Ion exchange membrane
Permselectivity
Membrane potential
Donnan equilibrium
Manning theory

ABSTRACT

Electrodialysis, reverse electrodialysis, and related electrochemical processes are increasingly important technologies for water purification and renewable energy generation and storage. The electrical efficiency of these processes is directly related to the permselectivity of the ion exchange membranes (IEMs) – defined as the extent to which the membrane permits the passage of counter-ions (ions of opposite charge to the membrane, e.g., cations for a cation exchange membrane) while blocking passage of co-ions. Permselectivity is not a material constant, but rather depends on the concentration and composition of the electrolyte solutions in contact with the IEM. Thus, even though permselectivity is routinely measured at standardized conditions (usually 0.5 M/0.1 M NaCl or KCl), the practical utility of such data is limited because we lack an accurate, quantitative way of using it to predict permselectivity under relevant process conditions. Moreover, the concentration dependence of IEM permselectivity has historically been studied primarily by evaluating the performance of (reverse) electrodialysis stacks rather than individual membranes, which has made it difficult to relate the concentration dependence of permselectivity to specific membrane characteristics. In this study, we measured the permselectivity of four commercial IEMs in six different concentration gradients employing 4 M and 0.5 M NaCl as the high salt concentration. We then constructed a predictive model of membrane permselectivity based on the extended Nernst-Planck equation and investigated how accounting for convection and electrostatic effects (via Manning's counter-ion condensation theory) affected model accuracy. We demonstrate that accurate, quantitative predictions of IEM permselectivity as a function of external salt concentrations are possible and require knowledge of only four easily measured membrane properties: water uptake, water permeability, charge, and thickness.

1. Introduction

Electrodialysis, reverse electrodialysis, and related electrochemical processes are increasingly important technologies for water purification and renewable energy generation and storage [1–5]. In such processes, the current efficiency is directly related to the permselectivity of the ion exchange membranes (IEMs) – defined as the extent to which the membrane permits the passage of counter-ions (ions of opposite charge to the membrane, e.g., cations for a cation exchange membrane) while blocking passage of co-ions [6].

Permselectivity is not a material constant, but rather depends on the concentration and composition of the electrolyte solutions in contact with the membrane [7–11]. In general, the permselectivity of IEMs is highest at low to moderate salt concentrations, and decreases when the membranes are exposed to high salt concentrations due to charge screening and the suppression of Donnan exclusion [3,7,8,12,13]. Permselectivity is typically reported by IEM manufacturers under standard conditions (usually 0.5 M/0.1 M NaCl or KCl), but the practical utility of such data is limited because we lack an accurate, quantitative way of using it to predict permselectivity under actual process conditions. Such predictive capability is important for evaluating new applications of (reverse) electrodialysis that involve higher salt concentrations, such as recovery of valuable products from desalination brine [4,14–16], hypersaline RED [3,4,17–21], heat recovery [22–24], or energy storage [25–27]. Moreover, an accurate understanding of the concentration dependence of IEM permselectivity, and of which

* Corresponding author.
E-mail address: coronell@unc.edu (O. Coronell).

https://doi.org/10.1016/j.memsci.2020.118411
Received 4 February 2020; Received in revised form 3 June 2020; Accepted 17 June 2020
Available online 29 June 2020

membrane properties determine this dependency, is essential to developing membranes with more robust performance.

To date, the concentration dependence of IEM permselectivity has been studied primarily by evaluating the performance of (reverse) electrodialysis stacks rather than individual membranes. Several theoretical [7,13,28] and experimental [8,19,21,29,30] studies have shown that the decrease in membrane permselectivity at high salt concentrations has a significant detrimental effect on stack performance, and a few studies [7,13,19,28,31] have presented empirical or semi-empirical models that predict stack performance over a range of salt concentrations. Other models [7,32,33] were based on fundamental ion transport theory, but made limiting assumptions, such as neglecting convection or assuming that the AEM and the CEM had identical properties. All these modeling studies have used stack data (i.e., the performance of an AEM and CEM pair) for calibration, making it difficult to examine relationships between specific membrane properties and permselectivity.

Thus, the literature contains very little data on the concentration dependence of permselectivity of individual IEMs, especially when exposed to high salt concentrations. One exception is an experimental study by Zlotorowicz et al. [29], which measured the permselectivity of individual AEMs and CEMs over a range of salt concentrations. However, this work studied only small concentration gradients, and the maximum salt concentration was 0.5 M, which gives the study limited relevance to more challenging ED/RED process conditions. Furthermore, no studies of which we are aware have compared the permselectivity of different types of AEMs or CEMs exposed to multiple salt concentrations and related their performance to membrane properties via a fundamental ion transport model.

Accordingly, our objectives in this study were to 1) measure the permselectivity of multiple IEMs in several concentration gradients involving high salt concentrations, 2) relate the observed permselectivity (and its concentration dependence) to individual membrane properties, and 3) develop a quantitative method to predict the permselectivity of IEMs as a function of membrane properties and external salt concentrations. To accomplish these objectives, we measured the permselectivity of two AEMs and two CEMs whose properties were comprehensively characterized in our previous work [34], exposing them to six concentration gradients employing 4 M and 0.5 M NaCl as the high salt concentration. We constructed a predictive model of membrane permselectivity based on the extended Nernst-Planck equation, and then investigated how accounting for 1) convection, 2) electrostatic effects (via Manning's counter-ion condensation theory), and 3) the shape of the concentration profile within the membrane affected model accuracy. Our analysis contributes to a clearer understanding of the connection between individual membrane properties and selective ion transport in IEMs and suggests specific design strategies for IEMs used in high-salinity applications.

2. Origins of permselectivity and electric potential in ion exchange membranes

2.1. System of interest

The system of interest in this study is a charged polymer membrane separating two salt solutions of different concentration, as shown in Fig. 1. As long as the concentration of fixed charge groups inside the membrane exceeds the salt concentration in the external solution, the presence of fixed charge groups causes the concentration of counter-ions, $\bar{C}_{ct}$, to increase substantially compared to that in the bulk solution, while the co-ion concentration $\bar{C}_{co}$ is reduced. Due to the concentration gradient between the two solutions, counter-ions diffuse through the membrane, creating a slight charge imbalance that results in an electric potential, E_{mem}, across the membrane. For example, when the membrane in Fig. 1 is a CEM, cations diffuse from left to right, making the solution on the right slightly positive with respect to the solution on the left. The excess of positive charge creates a potential that transports cations in the opposite direction (right to left) until a steady-state between diffusion (left to right) and migration (right to left) is established [35].

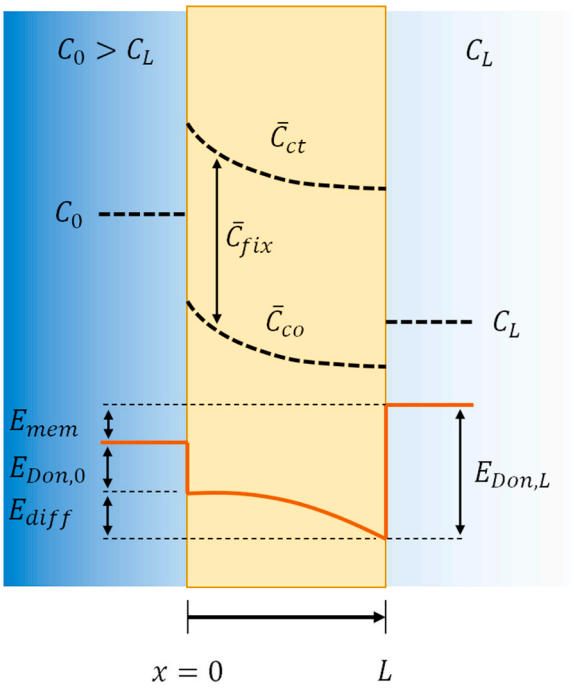

Fig. 1. Profiles of electric potential, counter-ion concentration, and co-ion concentration in an ion exchange membrane. Profiles are drawn to represent a cation exchange (negatively-charged) membrane.

2.2. Permselectivity

Ion exchange membrane permselectivity quantifies the extent to which the flux of electric charge (i.e., the current) through the membrane is carried by counter-ions. The fraction of electric current carried by a particular species is given by its transport number, t_i (dimensionless), which is defined as [36]

$$t_i = \frac{z_i J_i}{\sum_i z_i J_i} \tag{1}$$

where z (dimensionless) is the signed charge, J (mol.m^{-2}.s^{-1}) is the migration flux (i.e., the flux driven by an electric field), and subscript i indicates any species. By this definition, the sum of transport numbers over all species subject to migration is equal to 1, and $0 < t_i < 1$ for any individual species. In general, the transport numbers of the cation and anion in a salt (e.g., Na^+ and Cl^-) are not equal, due to differences in ion mobility. In a bulk solution, the more mobile ion carries a greater fraction of electric current than the less mobile one. In an IEM, the concentrations of the two ions are highly unequal, so the transport number is influenced both by ion mobility and by the respective concentrations. An ideally permselective IEM has a counter-ion transport number equal to 1, indicating that all current is carried by the counter-ion.

Permselectivity, α (dimensionless), is defined based on transport numbers as [6,35,36]

$$\alpha \equiv \frac{\bar{t}_{ct} - t_{ct}}{1 - t_{ct}}, \tag{2}$$

where $\bar{t}$ and t are the transport numbers in the membrane and bulk solution, respectively, and subscript ct denotes the counter-ion. Note that when $\bar{t}_{ct} = 1$, $\alpha = 1$, while $\alpha \to 0$ as $\bar{t}_{ct} \to t_{ct}$ (i.e., when the counter-ion has equal transport numbers in the membrane and bulk solution phases). The counter-ion transport number $\bar{t}_{ct}$ is affected by the ion concentration, ion mobility, and rate of water transport through the membrane [29], as elaborated below.

The counter-ion transport number in the membrane ($\bar{t}_{ct}$) can be determined by measuring counter-ion and co-ion fluxes through an IEM at different levels of applied current. Although this "dynamic" method (also known as the Hittorf method) provides a direct measurement of $\bar{t}_{ct}$, it is time-consuming, affected by boundary layer effects such as concentration polarization, and requires extrapolating results to open circuit conditions [29,36,37]. $\bar{t}_{ct}$ is more commonly measured using a rapid, "static" method based on the open-circuit membrane potential, E_{mem} (mV). However, certain simplifying assumptions (discussed below) must be made to calculate $\bar{t}_{ct}$, from E_{mem}. As such, permselectivity values obtained from membrane potential measurements slightly underestimate the true permselectivity given in Eq. (2), and hence are termed "apparent permselectivity" [7,29,36,38,39]. Apparent permselectivity measurements also differ from the true permselectivity under operating conditions because, by definition, apparent permselectivity is measured in the absence of an electric current and does not include the effect of concentration gradients parallel to the membrane. Nevertheless, apparent permselectivity is a useful measure of selective ion transport, and represents the measure that is most widely-reported in ion exchange literature. In the remainder of this work, our use of the term "permselectivity" always refers to apparent permselectivity.

2.3. Membrane potential

The membrane potential arises from selective ion transport when an IEM separates two electrolyte solutions of different concentration, as explained above (see Fig. 1). This membrane potential comprises two equilibrium Donnan potentials, E_{Don}, and a diffusion potential, E_{diff}, and is given by [35,40]

$$E_{mem} = E_{Don,0} + E_{diff} - E_{Don,L}, \tag{3}$$

where subscripts 0 and L represent the high-concentration and low-concentration interfaces of the IEM, respectively (see Fig. 1). Defined in this way, E_{mem} represents the potential of the more dilute solution ($x = L$) with respect to the more concentrated one ($x = 0$), as indicated in Fig. 1. As can be deduced from the definitions of E_{Don} (Eq. (4)) and E_{diff} (Eq. (5)) below, a cation exchange membrane will have a positive E_{mem}. This is consistent with the fact that when cations diffuse to the low-concentration side through a cation exchange membrane, the dilute solution becomes more positive than the concentrated one.

The Donnan potentials arise from differences in the thermodynamic activity of the counter-ions in the membrane and bulk solution phases, and are given by [11,35,36,41]

$$E_{Don} = -\frac{RT}{z_{ct}F}\ln\frac{\bar{a}_{ct}}{a_{ct}}, \tag{4}$$

where and $\bar{a}_{ct}$ and a_{ct} (dimensionless) are the activities of the counter-ion in the membrane and bulk solution, respectively, R (8.314 J mol^{-1} K^{-1}) is the ideal gas constant, T (K) is the temperature, and F (96,485 C mol^{-1}) is the Faraday constant. Note that Eq. (4) can also be written in terms of co-ion activities with equivalent results [11].

The diffusion potential arises from differences in the mobility of the counter-ion and co-ion inside the membrane. In this work, we obtained an expression for the diffusion potential by integrating the extended Nernst-Planck flux equations for the counter-ion and co-ion over the membrane thickness, including the effects of convection (see Supplementary Material). Although the Nernst-Planck model formulation makes several simplifying assumptions (for example, it neglects ion-ion interactions and assumes that ion mobility is proportional to ion diffusion coefficient), it has been widely used in the ion exchange literature with good results [4]. The resulting expression for a solution containing one binary salt (one anion and one cation) is

$$E_{diff} = -\frac{RT}{F}\left[\sum_i \int_{x=0}^{L} \frac{\bar{t}_i}{z_i} d\ln\bar{a}_i + \frac{\Delta P - \Delta\pi}{L}\int_{x=0}^{L} \frac{\bar{t}_w}{RTz_{fix}\bar{C}_{fix}} dx\right], \tag{5}$$

where

$$\bar{t}_i = \frac{z_i^2\bar{D}_i\bar{C}_i}{z_{ct}^2\bar{D}_{ct}\bar{C}_{ct} + z_{co}^2\bar{D}_{co}\bar{C}_{co} + RTz_{fix}^2P_w^H\bar{C}_{fix}^2}, \tag{6}$$

and

$$\bar{t}_w = \frac{RTz_{fix}^2P_w^H\bar{C}_{fix}^2}{z_{ct}^2\bar{D}_{ct}\bar{C}_{ct} + z_{co}^2\bar{D}_{co}\bar{C}_{co} + RTz_{fix}^2P_w^H\bar{C}_{fix}^2}, \tag{7}$$

where ΔP and $\Delta\pi$ (bar) are the differences in hydraulic and osmotic pressures, respectively, between the two external solutions, $\bar{t}_i$ (dimensionless) is the ion transport number, $\bar{t}_w$ (dimensionless) is the transport number of water, P_w^H (m^2.s^{-1}.Pa^{-1}) is the hydraulic water permeability of the membrane, equal to the water permeance A (L.m^{-2}.hr^{-1}.bar^{-1}) times membrane thickness L (and independent of position in the membrane), the index i indicates a summation over the ionic species, and subscript co denotes the co-ion. For the conditions considered here (and in most electrochemical membrane processes), $\Delta P = 0$.

The water transport number, $\bar{t}_w$, can be interpreted as follows. In an IEM, the liquid inside the membrane is not electroneutral due to the excess of counter-ions over co-ions (macroscopic electroneutrality is maintained by the presence of the fixed charge groups attached to the membrane; see Eq. (21)). Therefore, any movement of water through the membrane imparts greater momentum to counter-ions than to co-ions, and results in a movement of electric charge (the "streaming current") [35]. Thus, $\bar{t}_w$ represents the electric current (i.e., charge flux) carried by water divided by the total migration flux, consistent with the definition of transport numbers we presented in Eq. (1). Note that under open circuit conditions the net electrical current is zero, meaning that the ionic flux due to diffusion is exactly balanced by the combined flux due to migration and the streaming current.

The left-hand term inside the brackets in Eq. (5) is the expression for diffusion potential commonly found in literature [6,11,35,42], which neglects convection through the membrane. Models of ion transport in IEMs are often based on the classical Nernst-Planck equation, which considers only diffusion and migration and neglects convection [7,32,40]. This omission is justified by the relatively low water permeance of IEMs and the fact that, when an electric current is applied, migration flux is usually much larger than convection flux [12]. However, convection is known to reduce the membrane potential [29,33,35], and is especially likely to be relevant in this work, given the large concentration gradients and open-circuit conditions we employed. Even for small concentrations and concentration gradients, Zlotorowicz et al. [29] showed that deviations from ideal permselectivity normally attributed to co-ion transport could actually be explained by water transport through the membrane. Thus, we include convection when calculating the diffusion potential.

Substituting Eq. (4) and Eq. (5) into Eq. (3) yields the overall expression for the membrane potential

$$E_{mem} = -\frac{RT}{z_{ct}F}\ln\frac{\bar{a}_{ct,0}a_{ct,L}}{a_{ct,0}\bar{a}_{ct,L}} - \frac{RT}{F}\left[\sum_i \int_{x=0}^{L} \frac{\bar{t}_i}{z_i} d\ln\bar{a}_i + \frac{\Delta P - \Delta\pi}{L}\int_{x=0}^{L} \frac{\bar{t}_w}{RTz_{fix}\bar{C}_{fix}} dx\right]. \tag{8}$$

By definition, the summation of the transport numbers is equal to

one. Thus, when there is only one counter-ion and one co-ion (i.e., for a binary salt), $\bar{t}_{ct} + \bar{t}_{co} + \bar{t}_w = 1$, which allows us to rewrite Eq. (8) as

$$E_{mem} = -\frac{RT}{z_{ct}F}\ln\frac{a_{ct,L}}{a_{ct,0}} - \frac{RT}{F}\left[-\int_{x=0}^{L}\frac{\bar{t}_{co}}{z_{ct}}d\ln\bar{a}_{ct} + \int_{x=0}^{L}\frac{\bar{t}_{co}}{z_{co}}d\ln\bar{a}_{co} - \int_{x=0}^{L}\frac{\bar{t}_w}{z_{ct}}d\ln\bar{a}_{ct} + \frac{\Delta P - \Delta\pi}{L}\int_{x=0}^{L}\frac{\bar{t}_w}{RTz_{fix}\bar{C}_{fix}}dx\right], \tag{9}$$

In the case of perfect permselectivity, in which $\bar{t}_{co} = 0$ and $\bar{t}_w = 0$, the terms in bracket vanish, and the left hand terms simplifies to the well-known Nernst equation:

$$E_{mem} = -\frac{RT}{z_{ct}F}\ln\frac{a_{ct,L}}{a_{ct,0}} \approx -\frac{RT}{z_{ct}F}\ln\frac{a_{\pm,L}}{a_{\pm,0}} = E_{mem,ideal}, \tag{10}$$

where $a_\pm$ is the mean ion activity, which we use to approximate a_{ct} since single-ion activities in bulk solution cannot be measured. Hence, the left-hand term in Eq. (9) represents the maximum attainable value of the membrane potential ($E_{mem,\ ideal}$), while the terms in brackets represent the deviation from ideal behavior due to co-ion transport and convection. Note that if we remove the effects of convection (remove the terms containing $\bar{t}_w$) and make the substitution $\bar{a}_\pm = \sqrt{\bar{a}_{co}\bar{a}_{ct}}$, Eq. (9) is equivalent to Eq. 8-77 presented by Helfferich [35], which presents a rigorous derivation of the membrane potential excluding the effects of convection.

In order to calculate $\bar{t}_{ct}$ from measurements of E_{mem} as is routinely done in apparent permselectivity experiments, several simplifications to Eq. (9) are made. First, for the special case of a symmetrical electrolyte (e.g., NaCl, $CaSO_4$, etc.), assuming that the transport numbers throughout the membrane are constant, Eq. (9) is simplified (see Supplementary Material) to

$$E_{mem} = -(2\bar{t}_{ct} - 1 + \bar{t}_w)\frac{RT}{z_{ct}F}\ln\frac{a_{\pm,L}}{a_{\pm,0}} - \bar{t}_w\left(\frac{(\Delta P - \Delta\pi)}{z_{fix}F\bar{C}_{fix}}\right). \tag{11}$$

Note that in making this simplification, we replaced individual membrane-phase ion activities $\bar{a}_{ct}$ and $\bar{a}_{co}$ with the mean membrane-phase ion activity $\bar{a}_\pm$, which in turn was replaced by the mean solution-phase activity $a_\pm$. The substitution of $a_\pm$ for $\bar{a}_\pm$ is exact when applied to the mobile salt (but not to individual ions), because the total electrochemical potential of any species is continuous across a phase boundary and for a symmetrical mobile salt (i.e., a cation-anion pair), the electrostatic contributions to electrochemical potential cancel one another, so that $\ln\frac{\bar{a}_{\pm,L}}{\bar{a}_{\pm,0}} = \ln\frac{a_{\pm,L}}{a_{\pm,0}}$ [35,41,42,43].

Second, the water transport number is assumed to be zero for the reasons discussed above, which results in the following further simplification of Eq. (11):

$$E_{mem} = -(2\bar{t}_{ct} - 1)\frac{RT}{z_{ct}F}\ln\frac{a_{\pm,L}}{a_{\pm,0}}. \tag{12}$$

Eq. (12) can be used to obtain $\bar{t}_{ct}$ from E_{mem} as

$$\bar{t}_{ct} = \frac{\frac{E_{mem}}{E_{mem,ideal}} + 1}{2}. \tag{13}$$

These equations are commonly reported in literature [11,36,37], and are the basis for the calculation of apparent permselectivity, α_{app}, which is obtained by inserting Eq. (13) into Eq. (2):

$$\alpha_{app} = \frac{\frac{E_{mem}}{E_{mem,ideal}} + 1 - 2t_{ct}}{2t_{co}}. \tag{14}$$

In many cases, apparent permselectivity is measured with the membrane in a salt in which $t_{ct} \approx t_{co} \approx 0.5$ (such as KCl), in which case $\alpha_{app} \approx \frac{E_{mem}}{E_{mem,ideal}}$ [36]. Many studies in literature employ this approximation. We employ the non-approximated expression for apparent permselectivity (Eq. (14)) in all calculations in this work.

3. Predictive model of apparent membrane permselectivity

3.1. Overview of modeling approach

The equations presented in the previous section illustrate that in order to predict apparent permselectivity (α_{app}), it is necessary to predict E_{mem} (Eq. (12)). Calculation of E_{mem} (Eq. (9)) requires knowledge of the transport numbers and activities of both counter- and co-ions as a function of position in the membrane, as well as the water transport number. In this section, we describe a stepwise approach to calculating each of these quantities, making use of Donnan-Manning theory and the Mackie-Meares diffusion model. A conceptual view of the required inputs and resulting outputs of our model is given in Fig. 2. Briely, based on membrane characteristics such as water uptake and charge concentration, we first solve for the ion concentrations at each interface and then calculate other quantities (e.g., ion concentration, activity and diffusion profiles) as a function of position in the membrane by assuming a linear concentration profile. These quantities are then used to solve for the membrane potential and apparent permselectivity as described in detail in the following sections.

3.2. Interface concentrations

The first step in the calculation is to determine the ion concentrations just inside the membrane at each interface. At the interfaces between the membrane and bulk solutions, ions partition into the membrane in such a way that their electrochemical potential is the same in both phases [35,41,42,43]. Mathematically, this condition is expressed by equating the electrochemical potential of the ions in both phases as follows:

$$\bar{a}_{co}^{\nu_{co}}\bar{a}_{ct}^{\nu_{ct}} = a_{co}^{\nu_{co}}a_{ct}^{\nu_{ct}} \tag{15}$$

and

$$a = \gamma C, \tag{16}$$

where C (M) is the ion concentration, γ is the activity coefficient, and ν is the stoichiometric dissociation coefficient for the salt ($\nu_+ = \nu_- = 1$ for NaCl). Overbars indicate the membrane phase. Combining Eqs. (15) and (16) gives

$$\left(\bar{\gamma}_{co}\bar{C}_{co}\right)^{\nu_{co}}\left(\bar{\gamma}_{ct}\bar{C}_{ct}\right)^{\nu_{ct}} = (\gamma_{co}C_{co})^{\nu_{co}}(\gamma_{ct}C_{ct})^{\nu_{ct}}. \tag{17}$$

Since it is impossible to measure individual ion activity coefficients in bulk solution, we rewrite Eq. (17) in terms of the mean ionic activity coefficient, $\gamma_\pm$, and the salt concentration, C_s, which are defined as [44].

$$\gamma_\pm = \left(\gamma_{ct}^{\nu_{ct}}\gamma_{co}^{\nu_{co}}\right)^{\frac{1}{\nu_{ct}+\nu_{co}}} \tag{18}$$

and

$$C_s = \frac{C_{co}}{\nu_{co}} = \frac{C_{ct}}{\nu_{ct}}, \tag{19}$$

respectively. Substituting Eqs. (18) and (19) into Eq. (17) gives

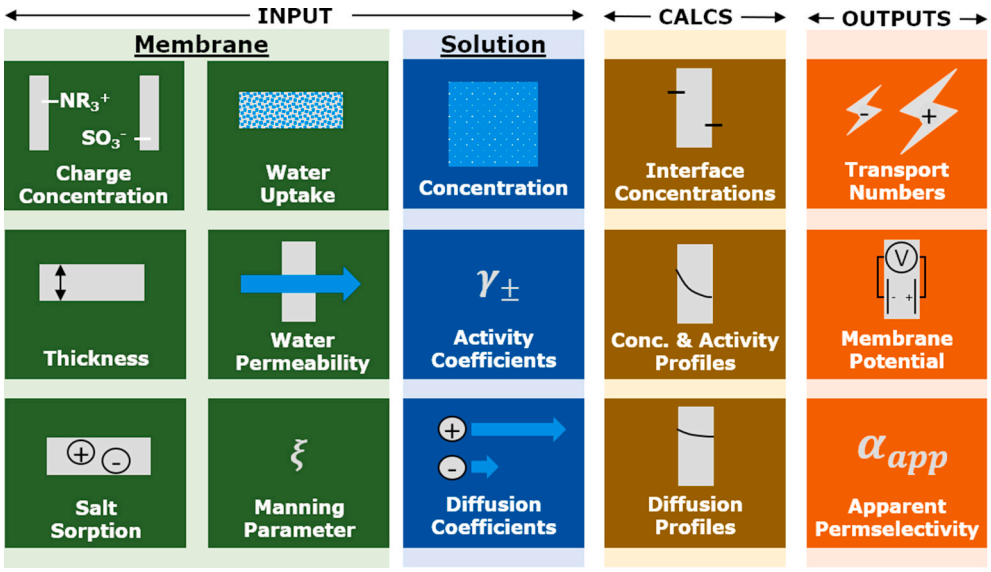

Fig. 2. Conceptual overview of predictive model for membrane potential and apparent permselectivity.

$$(\overline{\gamma}_{co}\overline{C}_{co})^{\nu_{co}}(\overline{\gamma}_{ct}\overline{C}_{ct})^{\nu_{ct}} = \nu_{ct}^{\nu_{ct}}\nu_{co}^{\nu_{co}}(\gamma_\pm C_s)^{\nu_{ct}+\nu_{co}}. \quad (20)$$

Next, we consider the influence of the fixed charge on the IEMs. Local electroneutrality must prevail at all locations in the membrane phase, so that

$$z_{ct}\overline{C}_{ct} + z_{co}\overline{C}_{co} + z_{fix}\overline{C}_{fix} = 0, \quad (21)$$

where z_{fix} (dimensionless) and $\overline{C}_{fix}$ (mol.L^{-1} water sorbed) are the signed charge number and concentration of fixed ionic groups in the membrane, respectively. By definition, the co-ion and the fixed charge sites have the same sign. Combining Eq. (20) and Eq. (21) and solving for $\overline{C}_{co}$ yields

$$\overline{C}_{co}^{\ \nu_{co}}\left(\frac{z_{co}\overline{C}_{co} + z_{fix}\overline{C}_{fix}}{z_{ct}}\right)^{\nu_{ct}} = -\Gamma\nu_{ct}^{\nu_{ct}}\nu_{co}^{\nu_{co}}(C_s)^{\nu_{ct}+\nu_{co}}, \quad (22)$$

where

$$\Gamma = \frac{\gamma_\pm^{(\nu_{ct}+\nu_{co})}}{\overline{\gamma}_{ct}^{\ \nu_{ct}}\overline{\gamma}_{co}^{\ \nu_{co}}}. \quad (23)$$

In the case of a monovalent, 1:1 salt (e.g., NaCl) where $|z_{fix}| = 1$, Eq. (22) can also be expressed as [35,43,45,46]

$$\overline{C}_{co} = C_s\sqrt{\Gamma}\sqrt{\left(\frac{\overline{C}_{fix}}{2C_s\sqrt{\Gamma}}\right)^2 + 1} - \frac{\overline{C}_{fix}}{2C_s\sqrt{\Gamma}} = C_s\sqrt{\Gamma}\exp\left(-\operatorname{asinh}\frac{\overline{C}_{fix}}{2C_s\sqrt{\Gamma}}\right). \quad (24)$$

Eq. (22) or (24), known as the Donnan equilibrium, provides a way to calculate the membrane-phase co-ion concentration in equilibrium with a bulk electrolyte solution. Typically, C_s is known and $\overline{C}_{fix}$ can be easily measured or calculated from information in membrane specifications. In the "ideal" Donnan model, $\Gamma = 1$, implying that both the bulk electrolyte solution and the ions inside the membrane behave as ideal solutions, or equivalently, that their activity coefficients inside and outside of the membrane are the same [43,45]. Alternatively, as in this work, Manning's counter-ion condensation theory, elaborated below, can be used to calculate $\overline{\gamma}_{ct}$ and $\overline{\gamma}_{co}$, while $\gamma_\pm$ can be obtained from literature or calculated from, e.g., the Pitzer model [47,48]. Thus, $\overline{C}_{co}$ is the only unknown in Eq. (22) or Eq. (24). After obtaining $\overline{C}_{co}$, we obtained the interface counter-ion concentration, $\overline{C}_{ct}$, by using Eq. (21)).

3.3. Concentration profile

Having obtained the interface concentrations, we next calculated the ion concentrations as a function of position in the membrane using an empirical equation to represent the shape of the concentration profile. We discretized the membrane thickness into 25 slices, calculated $\overline{C}_{co}$ at the midpoint of each, and obtained the corresponding counter-ion concentration, $\overline{C}_{ct}(x)$, by recognizing that every position in the membrane must be electroneutral (Eq. (21)). Since several experimental and theoretical studies [7,49–52] have found that the ion concentration profiles in IEMs are nonlinear and that convection can exaggerate the nonlinearity [49,52], we investigated the sensitivity of our results to the shape of the concentration profile using an empirical equation that can be given an arbitrary curvature (see Supplementary Material). We found that a linear concentration profile resulted in the lowest the root mean square error (RMSE, i.e. $\sqrt{\frac{\sum_n(\text{prediction}-\text{experiment})^2}{n}}$) for E_{mem} (5.3 mV), while RMSE increased to 6–7.7 mV when the curvature of the profile was varied in either direction. The R^2 values for E_{mem} were above 0.994 in all cases. Thus, the most accurate prediction of E_{mem} was obtained using a linear profile. Based on this sensitivity analysis, and seeking to minimize the number of empirical fitting parameters in our model, we adopted the linear concentration profile for all remaining calculations. We also compared results using 10, 25, and 50 slices and found that the RMSE and of the model predictions for E_{mem} changed by less than 0.001 units (<0.2%) between 25 and 50 slices; thus, we used 25 slices for all model runs.

3.4. Activity profiles

Once the membrane concentration profile was determined, we calculated ion activity coefficients in the membrane using Manning theory. The thermodynamic behavior of the IEM is captured by the dimensionless Manning Parameter, ξ, which characterizes the distribution of charges along the polymer backbone and can be measured through ion sorption experiments [41]. When $\xi > \frac{1}{|z_{ct}|}$, which was the case for all the membranes we studied (see Table 1), the activity coefficients of the counter-ion and co-ion, $\overline{\gamma}_{ct}$ and $\overline{\gamma}_{co}$, respectively, are

Table 1
Properties of ion exchange membranes used in this study.[a]

Membrane	Salt Conc. ($mol.L^{-1}$)	Thickness (μm)	Charge Concentration[b] ($mol.L^{-1}$ water absorbed)	Water Uptake (g H_2O. g^{-1} dry polymer)	Manning Parameter, ξ (−)	Water Permeability,[c] P_w^H (L.μ $m.m^{-2}.hr^{-1}.bar^{-1}$)	Contact Angle[d] (°)
AMX	0.5	135 ± <1	8.05 ± 0.49	0.18 ± 0.01	1.00 ± 0.07	0.46 ± 0.02	36.4 ± 1.5
	4	133 ± 1	8.98 ± 0.45	0.16 ± 0.01		0.29 ± <0.01	
CMX	0.5	172 ± 1	7.21 ± 0.22	0.25 ± 0.01	1.27 ± 0.06	0.56 ± 0.02	36.3 ± 1.5
	4	170 ± 4	7.94 ± 0.31	0.22 ± 0.01		0.35 ± 0.02	
FAS-30	0.5	41 ± 1	10.55 ± 0.75	0.20 ± 0.01	1.41 ± 0.1	0.35 ± 0.02	58.5 ± 2.8
	4	30 ± 1	17.30 ± 1.28	0.12 ± 0.01		0.13 ± 0.01	
FKE-30	0.5	32 ± <1	6.95 ± 0.15	0.22 ± <0.01	1.11 ± 0.08	0.30 ± 0.01	59.3 ± 2.9
	4	32 ± 1	12.08 ± 0.86	0.13 ± 0.01		0.08 ± 0.01	

[a] All properties were measured in sodium chloride solutions at room temperature.
[b] Calculated from the ion exchange capacity and the water uptake [63].
[c] Calculated as the product of water permeance A ($L.m^{-2}.hr^{-1}.bar^{-1}$) and thickness L (μm) [59].
[d] Contact angle was measured only with the membranes immersed in 4 M NaCl. These values are considered representative of membrane hydrophilicity at 0.5 M NaCl as well.

given by Ref. [41]:

$$\overline{\gamma}_{ct} = \frac{\frac{X}{\xi z_{ct}} + \nu_{ct} z_{ct}}{X + \nu_{ct} z_{ct}} \exp\left[- \frac{\frac{1}{2} X}{X + \xi z_{co} z_{ct} (\nu_{ct} + \nu_{co})} \right] \tag{25}$$

and

$$\overline{\gamma}_{co} = \exp\left[- \frac{\frac{1}{2} X \frac{z_{co}^2}{z_{ct}}}{X + \xi z_{co} z_{ct} (\nu_{ct} + \nu_{co})} \right], \tag{26}$$

where

$$X = \frac{\overline{C}_{co}}{\overline{C}_{fix}}. \tag{27}$$

Using Eq. (25)–(27), the counter-and co-ion activity coefficients in the membrane were calculated as a function of position by substituting the appropriate value of $\overline{C}_{co}$ at each location. All other variables in Eq. (25)–(27) are constants. Having obtained both the concentration and activity coefficients for the counter-ion and co-ion as a function of position in the membrane, we then calculated the activity profile as $\overline{a}_i = \overline{\gamma}_i \overline{C}_i$ (Eq. (16)).

3.5. Transport number and diffusion coefficient profiles

Ion transport numbers in the membrane are essential for calculating membrane potential, and depend on both concentration and diffusion coefficients (see Eq. (6)). We have already described how to calculate (via the interface concentrations and Eq. (21)) the concentrations as a function of x, but we still require a way to calculate the ion diffusion coefficients in order to calculate the transport number. In general, we can express the diffusion coefficient in the membrane as a multiple of the value in bulk solution (D=1.334 × 10^{-9} and 2.032 × 10^{-9} m^2 s^{-1} for Na^+ and Cl^-, respectively [53]) as [54]

$$\frac{\overline{D}}{D} = f_{steric} f_{electric}, \tag{28}$$

where $f_{electric}$ and f_{steric} represent the effects of electrostatic interactions and tortuosity, respectively, on the diffusion coefficient in the membrane. f_{steric} can be estimated from the volume fraction of water in the membrane, φ_w (dimensionless), according to the Mackie-Meares model as [54–56]

$$f_{steric} = \left(\frac{\varphi_w}{2 - \varphi_w} \right)^2. \tag{29}$$

Note that according to Eq. (29), f_{steric} is the same for both the counter-ion and co-ion. In other words, the ratio of counter-ion to co-ion mobility in the membrane is the same as that in bulk solution.

To estimate the effect of electrostatic interactions on ion diffusion coefficients, we again turned to Manning theory. Kamcev et al. [54] developed the following equations to predict $f_{electric}$ for counter- and co-ions in charged polymer membranes [54,57]:

$$f_{electric,ct} = \frac{\frac{1}{|z_{ct}|\xi} X + |z_{ct}| \nu_{ct}}{X + |z_{ct}| \nu_{ct}} \left(1 - \frac{1}{3} z_{ct}^2 A\left(\frac{1}{|z_{ct}|}; \frac{X}{|z_{ct}|\xi} \right) \right), \tag{30}$$

$$f_{electric,co} = \left(1 - \frac{1}{3} z_{co}^2 A\left(\frac{1}{|z_{ct}|}; \frac{X}{|z_{ct}|\xi} \right) \right), \tag{31}$$

and

$$A\left(\frac{1}{|z_{ct}|}; \frac{X}{|z_{ct}|\xi} \right) = \sum_{m_1=-\infty}^{\infty} \sum_{m_2=-\infty}^{\infty} \left[\pi |z_{ct}| (m_1^2 + m_2^2) + |z_{ct}| + \frac{(\nu_{ct} + \nu_{co}) |z_{ct} z_{co}| |z_{co}| \xi}{X} \right]^{-2} \tag{32}$$

where the above equations apply when $\xi > \frac{1}{|z_{ct}|}$ and subscripts ct and co indicate the counter-ion and co-ion, respectively, as before. In contrast to the Mackie-Meares model for f_{steric}, the Manning model represented by Eqs. (30)–(32) predicts a change in the relative diffusivities of the counter-ion and co-ion. Similarly to Eqs. (25)–(27) for activity coefficients, the diffusion coefficients can be computed as a function of position by supplying the appropriate value of $\overline{C}_{co}$, which enters Eqs. (30) and (31) via the parameter X (see Eq. (27)). Transport numbers are then calculated from $\overline{D}$ and $\overline{C}$ according to Eq. (6).

3.6. Membrane potential and apparent permselectivity

Once the transport number and activity profiles throughout the membrane thickness were known, the membrane potential was calculated by numerical integration of Eq. (9), and the apparent permselectivity calculated via Eq. (14).

In the sections that follow, we evaluate the accuracy of this model to predict the membrane potential and apparent permselectivity of four IEMs exposed to a range of different salt concentrations. We already determined that the ion concentration profile shape within the membrane does not significantly affect predicted E_{mem} and apparent permselectivity results, as discussed above. We now seek to better understand the relative significance of convection and non-ideal ion behavior. To do so, we evaluate two simplifications to the model: i) neglecting convection ($\bar{t}_w = 0$ in Eqs. (9) and (11)) and ii) assuming ideal behavior of ions (i.e., removing Manning theory from the model by setting $\Gamma = 1$ in Eq. (22) and $f_{electric} = 1$ in Eq. (28)).

4. Materials & methods

4.1. Ion exchange membranes

We tested two pairs of ion exchange membranes, each comprising one anion and one cation exchange membrane—Neosepta AMX and CMX and Fumatech FAS-30 and FKE-30, respectively. The two membrane pairs were chosen for their contrasting properties, summarized in Table 1. Properties in 4.0 M NaCl were reported previously [34,58], and properties in 0.5 M NaCl were obtained by the same techniques described in our previous work [34,58]. As shown in the table, the Neosepta membranes were relatively thick, hydrophilic, and contained reinforcing fabric, while the Fumatech membranes were thinner, more hydrophobic, and lacked reinforcement. The two membrane pairs exhibited other important contrasts in properties that will be discussed further in the Results and Discussion section. Here, we call attention to the fact that the fixed charge concentrations in all four membranes in 4.0 M NaCl (7.9–17.3 mol charge L^{-1} water absorbed) far exceed the external salt concentration. This fact is an important criterion for the effectiveness of Donnan exclusion. The extremely high fixed charge concentrations of the FAS and FKE membranes in particular can be explained by the large amount of osmotic deswelling exhibited by these membranes (Table 1), the implications of which we discuss further below.

Membrane coupons were immersed in sodium chloride solution to equilibrate for at least 24 h prior to testing. The concentration of the equilibration solution corresponded to the highest concentration to which the membranes would be exposed during measurement. All measurements reported herein represent the mean and standard error of at least three separate membrane coupons.

4.2. Apparent permselectivity

We measured apparent membrane permselectivity using the technique described in our previous work [60]. Briefly, circular membrane coupons (exposed area = 7.55 cm^2) were installed in a two-compartment cell (volume = 17 mL per compartment) containing sodium chloride solutions at various concentrations. The solutions were circulated through each side of the cell at a rate of approximately 50 mL min^{-1}, while the open-circuit membrane potential was measured by means of a pair of Ag/AgCl wires connected to a potentiostat (VMP3, Bio-Logic Science Instruments). The use of Ag/AgCl wires rather than single- or double-junction electrodes is important to prevent junction potentials from biasing the measurement [60], particularly in the case of large concentration gradients. The potential reading was deemed stable when its rate of change was less than 1.2 mV h^{-1}, after which we averaged the potential for 15 min and determined E_{mem} by correcting this average for the offset and concentration-dependent potentials of each pair of AgCl wires, as described previously [60].

The apparent permselectivity of each type of membrane was measured in sodium chloride solutions where the higher salt concentration (C_0) was either 0.5 M or 4 M, and the ratio of high to low concentration (C_0/C_L) was 5:1, 50:1, or 100:1 (six total conditions per membrane type). We chose C_0 = 0.5 M or 4 M values to mimic seawater applications (e.g., desalination or reverse electrodialysis power generation from natural seawater) and hypersaline applications, respectively. Different membrane coupons were used for each test condition. To confirm that there were no appreciable concentration changes as a result of salt diffusion between the compartments, we took samples of the circulating electrolyte solution on the low-concentration side of the cell at the end of every test and compared their conductivity to that of freshly-prepared solution. The dilute solution conductivity at the end of the test was statistically indistinguishable from the value at the beginning of the test (p = 0.05) in all cases but two, and in those cases the starting and ending conductivity values differed by less than 2%.

5. Results and Discussion

5.1. Experimental permselectivity

5.1.1. Permselectivity vs. concentration

Apparent permselectivity results are shown in Fig. 3. When C_0 was 0.5 M, all membranes had relatively high permselectivity, ranging from 0.937 to 0.985. Permselectivity was much lower when C_0 was 4.0 M, ranging from 0.647 to 0.918. For each value of C_0, the permselectivity increased as the value of C_L decreased. This trend was particularly evident in the results with C_0 = 4.0 M, where the permselectivity was 0.647–0.705 at C_L = 0.8 and increased to 0.805–0.918 at C_L = 0.04 M. These results illustrate that IEMs are able to maintain reasonably high permselectivity even at high values of C_0, provided that C_L is sufficiently low (for example, α_{app}>0.9 for C_L = 0.04 M). This finding is qualitatively consistent with previous experimental [8] and theoretical [7] studies which showed permselectivity to be more sensitive to the low salt concentration than the high salt concentration. Such behavior can be explained by considering the effectiveness of Donnan exclusion at each interface. Since Donnan exclusion becomes less effective as the adjacent bulk salt concentration increases (due to charge screening), the dilute solution interface at $x = L$ is always able to exclude co-ions more effectively than the concentrated solution interface at x = 0. Hence, the dilute interface has a particularly strong influence on the overall co-ion exclusion by the membrane, and thus the salt concentration adjacent to this interface has a particularly strong influence on permselectivity.

5.1.2. Permselectivity of AEMs vs. CEMs

Comparing the colors of the bars in Fig. 1a shows that the two CEMs were more selective than the AEMs under almost all conditions, with the differences being more pronounced at greater C_0. The higher selectivity of CEMs cannot be easily explained by any of the properties listed in Table 1. From the perspective of water uptake, charge, thickness, hydrophilicity, Manning parameter, or water permeability, each CEM is more similar to its corresponding AEM (e.g. CMX to AMX and FKE to FAS) than to the other CEM. The fact that differences in macroscopic membrane properties cannot explain the superior permselectivity of CEMs suggests that molecular-scale differences may play a significant role in determining permselectivity. One such likely important difference is the chemical interactions with sulfonate groups in CEMs vs. quaternary ammonium groups in AEMs. In a previous study of water

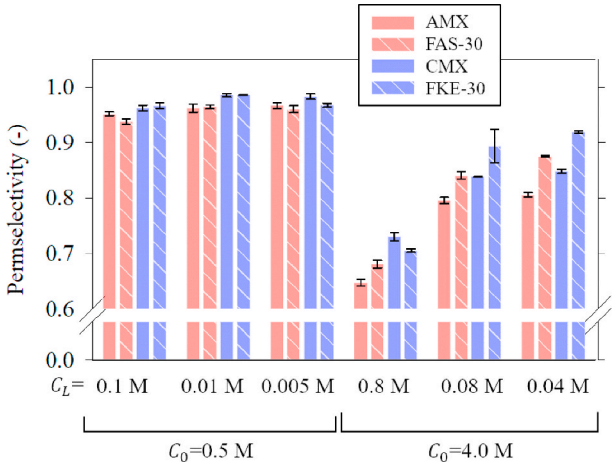

Fig. 3. Measured apparent permselectivity values. Red bars are anion exchange membranes; blue bars are cation exchange membranes (see legend). Error bars represent the standard error of at least three replicates. (For interpretation of the references to color in this figure legend, the reader is referred to the Web version of this article.)

uptake in 20 commercial IEMs [58] (including those used here), we observed evidence of stronger hydration of sulfonate groups than ammonium groups. Quantum mechanical simulations [61] and spectroscopy studies [62] also suggest differences in the hydration behavior of these groups.

5.1.3. Permselectivity of AMX vs. FAS and CMX vs. FKE

We next compare the permselectivity of the two AEMs (AMX vs. FAS) or the two CEMs (CMX vs. FKE). At $C_0 = 0.5\,M$, the permselectivity of AMX and FAS were comparable. However, at $C_0 = 4\,M$, FAS had a substantially higher permselectivity. Similar results were observed for the CEMs: CMX and FKE had similar permselectivities for $C_0 = 0.5\,M$, but when $C_0 = 4M$, FKE had a higher permselectivity in 2/3 cases ($C_L = 0.08$ and $0.04\,M$). Overall, the FAS/FKE membrane pair maintained higher permselectivity under high salt concentrations than the AMX/CMX membrane pair.

This difference in performance may be explained by differences in osmotic deswelling, which could affect the values of $\overline{C}_{fix}$ and the effectiveness of Donnan exclusion at each interface. The water uptake of FAS/FKE was much more sensitive to bulk salt concentration than that of AMX/CMX. For example, the water uptake of FAS decreased from 0.20 to 0.12 g $H_2O.g^{-1}$ membrane when C_0 increased from 0.5 to 4 M, causing $\overline{C}_{fix}$ to increase from 10.55 to 17.30 mol L^{-1}. By comparison, the water uptake of AMX membrane decreased from 0.18 to 0.16 g $H_2O.g^{-1}$ membrane, and $\overline{C}_{fix}$ increased from 8.05 to 8.98 mol L^{-1} (see Table 1). Thus, the higher permselectivity of FAS/FKE may be explained by the much higher value of $\overline{C}_{fix}$ at the high concentration interface, which would strengthen Donnan exclusion of co-ions. The greater sensitivity of FAS/FKE water uptake to external salt concentration than AMX/CMX is probably a consequence of the fact that the FAS/FKE membrane pair does not contain reinforcing material. As a result, increasing the external salt concentration causes greater osmotic deswelling, which dramatically increases $\overline{C}_{fix}$ in the FAS/FKE membrane pair.

The higher permselectivity of FAS/FKE when $C_0 = 4M$ may also be related to differences in water permeability. The FAS/FKE membranes had water permeability values that were roughly 1/2 to 1/3 those of the AMX/CMX, and these also showed strong concentration dependence, decreasing from 0.30 to 0.35 L.μm $m^{-2}.hr^{-1}.bar^{-1}$ at $C_0 = 0.5\,M$ to 0.08–0.13 L.μm $m^{-2}.hr^{-1}.bar^{-1}$ at $C_0 = 4M$. By contrast, the water permeabilities of the AMX/CMX pair were 0.46–0.56 and 0.29–0.35 L.μm $m^{-2}.hr^{-1}.bar^{-1}$ at $C_0 = 0.5M$ and $C_0 = 4M$, respectively. Water permeability of commercial IEMs is expected to decrease with decreasing water uptake [58], so the greater osmotic deswelling of the FAS/FKE pair also appears beneficial from the standpoint of limiting water permeability.

5.2. Predicted apparent permselectivity

Predicted values of apparent permselectivity, calculated according to the model presented above and the membrane properties given in Table 1, are compared with experimental results in Fig. 4a. Although there was a strong linear correspondence between the model predictions and experimental results ($R^2 = 0.926$, $p < 0.001$), the model generally underpredicted permselectivity. While its predictions were reasonably accurate for high permselectivity (e.g., $\alpha_{app} > 0.8$), they deviated from experimental values by as much as 40% in cases of lower permselectivity, with an overall RMSE of 0.086. The model predictions had

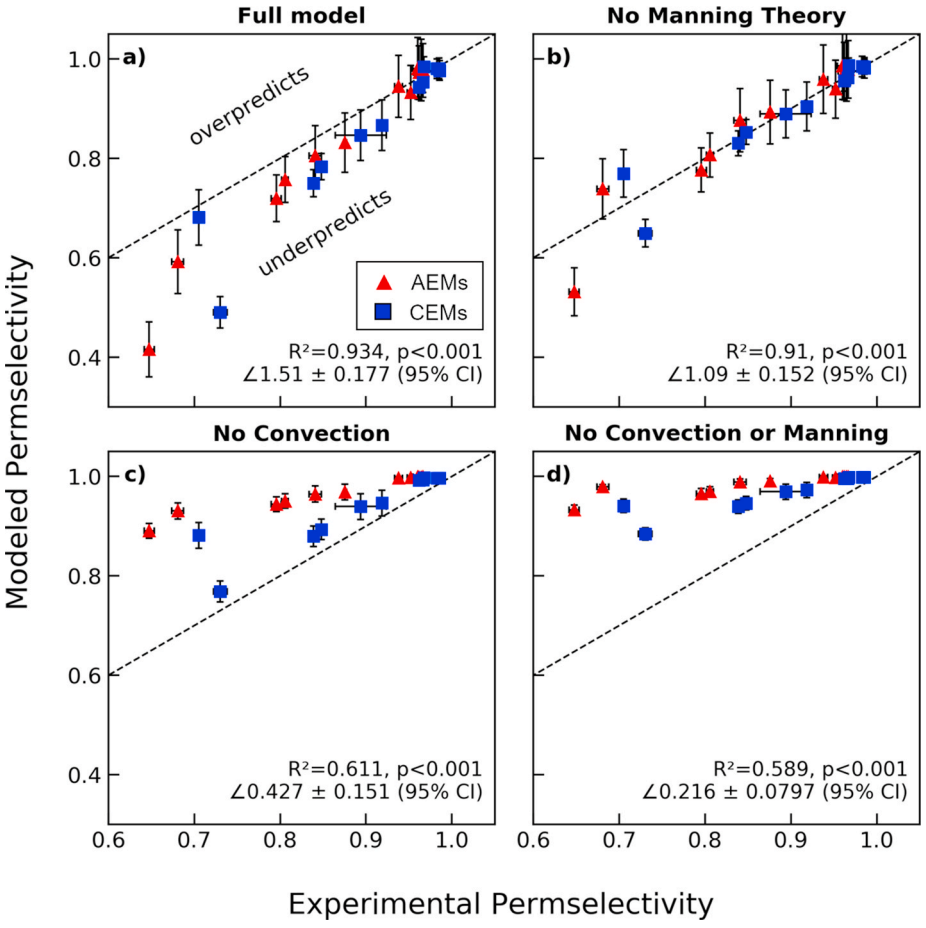

Fig. 4. Predicted vs. experimental apparent membrane permselectivity as calculated by a) the full model including Donnan and Manning theories and convection, b) the ideal Donnan model with convection but without Manning theory (i.e., $\Gamma = 1$ and $f_{electric} = 1$), c) the model including Donnan and Manning theories but neglecting convection effects ($\bar{t}_w = 0$ and $P_w^H = 0$), and d) the ideal Donnan model without Manning theory and neglecting convection effects. Red and blue symbols represent anion and cation exchange membranes, respectively. Dashed lines represent the line of perfect agreement between model and experiment. Error bars represent the propagated standard error associated with the experimental membrane properties given in Table 1. (For interpretation of the references to color in this figure legend, the reader is referred to the Web version of this article.)

similar accuracy for both AEMs and CEMs, as shown by comparing the positions of the red vs. blue data points in Fig. 4a.

Fig. 4b–d illustrate the accuracy of other scenarios involving modifications to the model. Removing Manning theory from the model (i.e., setting $\Gamma = 1$ in Eq. (22) and $f_{electric} = 1$ in Eq. (28), Fig. 4b) improved the accuracy of the predictions, reducing the RMSE to 0.038. Neglecting convection by setting $\bar{t}_w = 0$ in Eq. (9) and Eq. (11) (Fig. 4c) worsened the prediction considerably and caused the model to overpredict permselectivity in all cases, with an RMSE of 0.101. Finally, removing both Manning theory and convection from the model (Fig. 4d) resulted in the least accurate prediction overall, with an RMSE of 0.125. Additional quantitative results (e.g., R^2, p-value, RMSE, and absolute errors in permselectivity and membrane potential predictions) of these four scenarios as well as additional scenarios are shown in the Supplementary Material.

It is interesting to note that in the Manning theory scenario without convection (Fig. 4c), predicted values of apparent permselectivity were substantially more accurate for CEMs than for AEMs. To some degree, this may be a consequence of the unequal bulk solution transport numbers in Eq. (14) ($t_{Cl^-} > t_{Na^+}$), which cause the AEM permselectivity to be somewhat more sensitive to errors in membrane potential than CEM permselectivity (see Supplementary Material for a plot comparing the relative errors in E_{mem} and α_{app}). Consequently, a model scenario that predicts E_{mem} with equal accuracy for both types of membranes will inherently predict permselectivity in sodium chloride solutions less accurately for AEMs than CEMs. Thus, examining the accuracy of predictions of E_{mem} may explain the asymmetric accuracy in predictions of permselectivity that we see in Fig. 4c.

Among all the scenarios considered, the most accurate predictions of permselectivity were obtained by using the ideal Donnan model. Removing Manning theory from the model reduces the number of required membrane property inputs from six to four (Fig. 2). Thus, the predictive model we present here requires no adjustable parameters and only four IEM property measurements: the water uptake, ion exchange capacity, water permeance, and thickness (note that $\overline{C}_{fix}$ and water permeability P_w^H shown in Table 1 are calculated from water uptake and ion exchange capacity [63] and water permeance and thickness [59], respectively).

5.3. Predicted membrane potential

The finding that accounting for non-ideal behavior of ions inside the membrane via Manning's counter-ion condensation theory worsened the fit of the model to experimental data was surprising. To investigate the origins of this non-intuitive result, we now examine each of the key calculation steps leading to permselectivity, examining differences among the model scenarios. We begin with the predicted membrane potential.

To evaluate the accuracy of the membrane potentials predicted by the four model scenarios, we examine the predicted deviations from the ideal membrane potential ($E_{mem} - E_{mem,ideal}$). $E_{mem,ideal}$ appears in Eq. (9) and can be calculated exactly from the properties of the bulk solution, provided that sufficiently accurate values for the solution activity coefficients are available. Thus, accurately predicting E_{mem} really amounts to predicting how E_{mem} deviates from $E_{mem,ideal}$. The "deviation potentials" ($E_{mem} - E_{mem,ideal}$) are equivalent to the terms in brackets in Eq. (9), and represent the effects of imperfect counter-ion selectivity on E_{mem}. Moreover, since the apparent permselectivity of IEMs is relatively high (always greater than 60% in this work), the deviation potentials are a relatively small fraction of E_{mem}, Therefore, focusing on the deviation

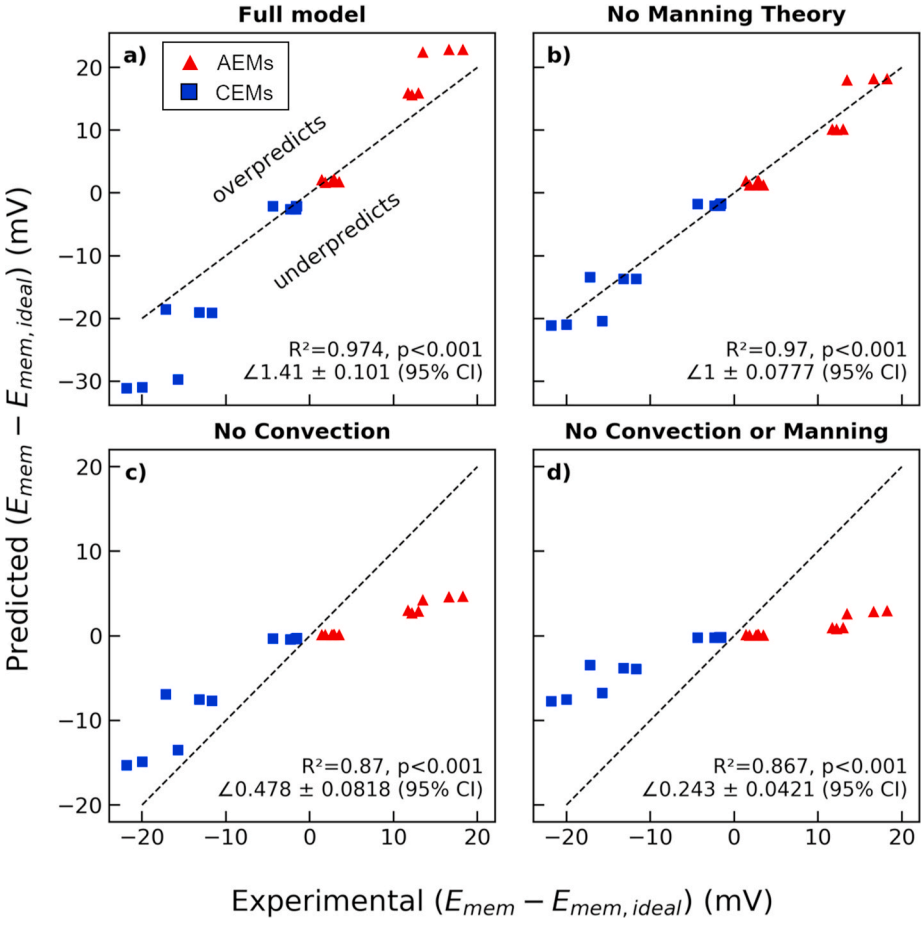

Fig. 5. Predicted vs. experimental deviations between the membrane potential E_{mem} and $E_{mem,ideal}$, as calculated by a) the full model including Donnan and Manning theories and convection, b) the ideal Donnan model with convection but without Manning theory (i.e., $\Gamma = 1$ and $f_{electric} = 1$), c) the model including Donnan and Manning theories but neglecting convection effects ($\bar{t}_w = 0$ and $P_w^H = 0$), and d) the ideal Donnan model without Manning theory and neglecting convection effects. Red and blue symbols represent anion and cation exchange membranes, respectively. Dashed lines represent the line of perfect agreement between model and experiment. Error bars (covered by the symbols in most cases) represent the propagated standard error associated with the experimental membrane properties given in Table 1. (For interpretation of the references to color in this figure legend, the reader is referred to the Web version of this article.)

potentials makes it easier to visualize differences in predictive accuracy between the model scenarios.

Predicted deviation potentials are shown in Fig. 5, where the slopes of the linear regressions between experimental and predicted deviation potentials give a quantitative measure of their relative accuracy. The full model had a slope of 1.41, indicating that it overpredicted deviations from $E_{mem,ideal}$. The two scenarios without convection had slopes of 0.48 and 0.24, indicating severe underprediction. The model without Manning theory (Fig. 5b) had a slope very close to 1, consistent with its accurate prediction of permselectivity observed in the previous section.

We note from the color of the data points that the deviation potentials for CEMs are all negative, while those for AEMs are positive. This is expected given that water and co-ion transport always reduce the magnitude of E_{mem}, which has opposite signs for CEMs (positive) and AEMs (negative). We also note that the magnitudes of the experimental deviations from $E_{mem,ideal}$ were similar for both AEMs and CEMs: up to ~20 mV in both cases. The values close to zero correspond to $C_0 = 0.5M$, where the membranes performed more ideally and had higher permselectivity, while the larger deviations correspond to $C_0 = 4M$.

The magnitudes of the *predicted* deviation potentials were generally similar for AEMs and CEMs, illustrated by the fact that the red and blue data points fell onto the same line. The only exceptions to this behavior were the predictions from the Manning model without convection (Fig. 5c). In that case, deviation potentials of up to ~15 mV were predicted for CEMs, while those for AEMs were ~5 mV or less, leading to red and blue data points clearly describing two lines with different slopes. We noted previously that asymmetry in the accuracy of predicted permselectivity between AEMs and CEMs (Fig. 4c) could be explained by the effect of the differences in bulk solution transport numbers between Na^+ and Cl^-. However, this rationale does not apply to predictions of E_{mem}. The fact that predicted values of E_{mem} were also less accurate for AEMs than CEMs in the Manning model without convection indicates that there is another source of asymmetry between AEMs and CEMs. Manning theory contains no ion specificity, and returns symmetric results (e.g. $\bar{\gamma}$, $f_{electric}$, etc.) for both cation and anion exchange membranes if their characteristics (ξ, $\overline{C}_{fix}$, φ_w) are the same. For the membranes in this work, the AEMs had a somewhat higher $\overline{C}_{fix}$ and lower φ_w than the CEMs, but these differences were not large enough to cause significant differences in the activity or diffusion coefficients predicted by Manning theory. Thus, the asymmetry in the predicted membrane potential of AEMs and CEMs was unexpected. We will explore its origins and implications further in a later section.

To continue investigating differences among the model scenarios, in Fig. 6, we decompose the predicted deviation potential $E_{mem} - E_{mem,ideal}$ into contributions from each of the terms in the deviation potential (see terms in brackets in Eq. (9)). Two of these terms represent the effects of convection and two represent the effects of co-ion transport on membrane potential. Note that all panels share a common scale on their y-axis. Comparing the panels, it is immediately obvious that the model scenarios without convection (panels c and d) predicted smaller deviation potentials than those with convection, consistent with the fact that they underpredicted the experimental deviation potentials. In the model scenarios with convection, it is also noteworthy that convection (red bars) appears to account for a majority of the deviation potentials even for $C_0 = 0.5\,M$. This is consistent with the conclusions of Zlotorowicz et al. [29] that deviations from ideal permselectivity in IEMs, even for small concentration differences, are attributable mainly to water transport rather than co-ion transport.

Comparing the model scenarios with and without convection (panels a and b vs. c and d) shows that, when convection is neglected, the predicted deviation potential due to co-ion transport is greater than when convection is not neglected. Since the sum of transport numbers must equal 1, and $\bar{t}_w = 0$ when convection is neglected, $\bar{t}_{ct}$ and $\bar{t}_{co}$ are both larger compared to the full model, and hence have a larger contribution

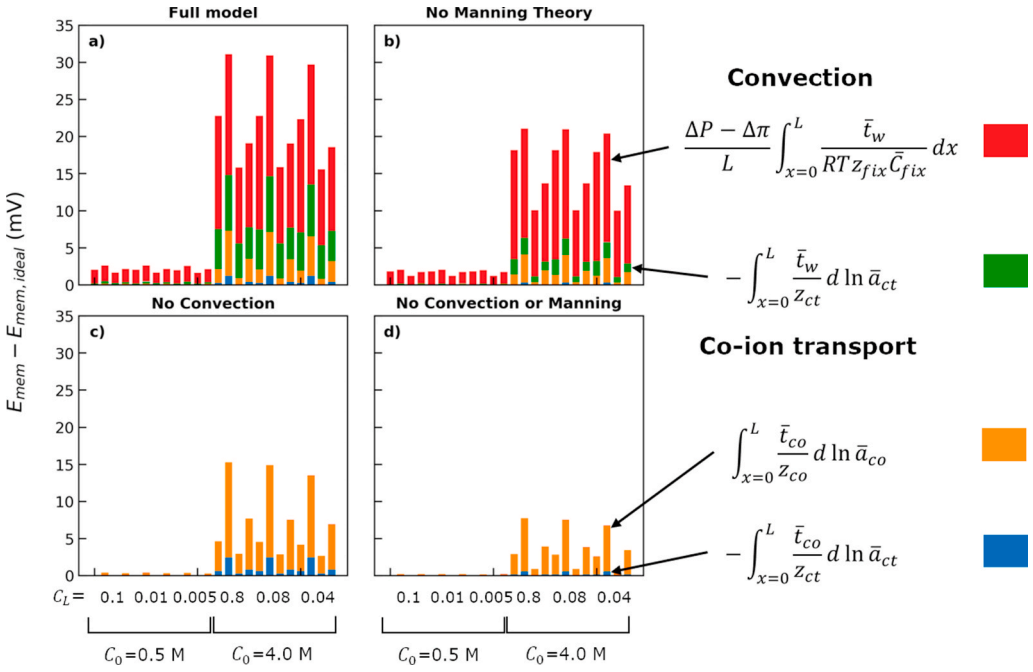

Fig. 6. Contribution of convection and co-ion transport to deviations from ideal membrane potential, as calculated a) the full model including Donnan and Manning theories and convection, b) the ideal Donnan model with convection but without Manning theory (i.e., $\Gamma = 1$ and $f_{electric} = 1$), c) the model including Donnan and Manning theories but neglecting convection effects ($\bar{t}_w = 0$ and $P_w^H = 0$), and d) the ideal Donnan model without Manning theory and neglecting convection effects.

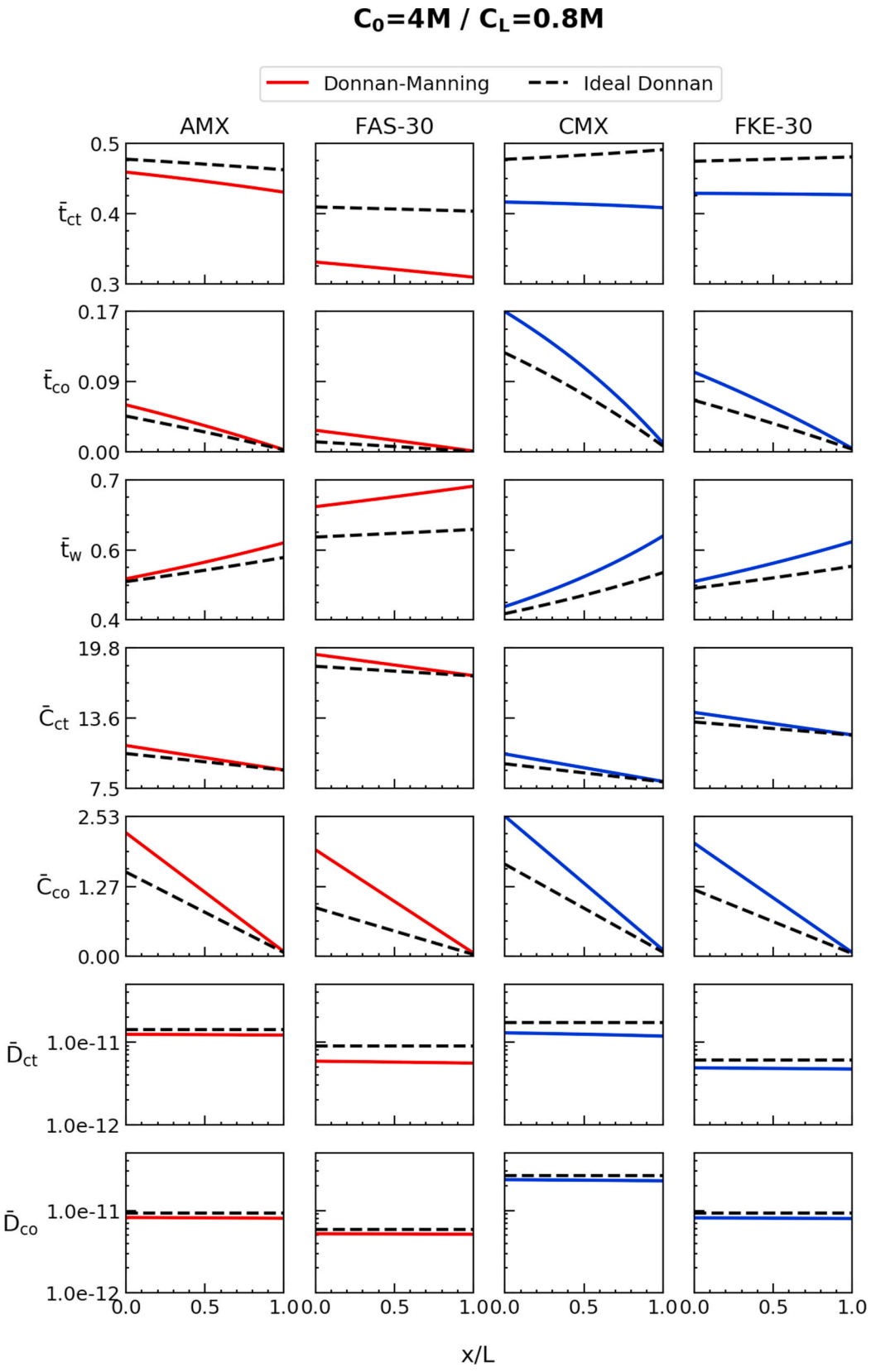

Fig. 7. Example concentration, diffusion coefficient, and transport number profiles for co-ions (subscript *co*) and counter-ions (subscript *ct*) in the membrane calculated via the full model including Donnan and Manning theories and convection (red or blue) or the ideal Donnan model with convection but without Manning theory (i.e., $\Gamma = 1$ and $f_{electric} = 1$, dashed lines). Each column represents one type of membrane. Profiles correspond to $C_0 = 4$ M and $C_L = 0.8$ M and are representative of most results. Profiles corresponding to other experimental conditions are provided in the Supplementary Material. (For interpretation of the references to color in this figure legend, the reader is referred to the Web version of this article.)

to the deviation potential. Thus, ion transport models that neglect convection may overestimate the effect of co-ion transport on membrane potential.

Comparing the scenarios with and without Manning theory (panels a and c vs. b and d) shows that the effects of both convection and co-ion transport are smaller (i.e., the red, green, and orange bars are all smaller) when Manning theory is not included in the model. This result can also be explained in terms of transport numbers. We show in the next section that the counter-ion transport number is larger in the model without Manning theory. As a result, both $\bar{t}_w$ and $\bar{t}_{co}$ have smaller values in these scenarios, and therefore have a smaller effect on the membrane potential (assuming activity profiles are relatively similar between scenarios).

5.4. Predicted transport number profiles

To understand why using Manning theory resulted in smaller predicted counter-ion transport numbers, in Fig. 7 we examine the calculated transport number profiles for model scenarios that include convection, with and without Manning theory. Since the counter-ion and co-ion transport numbers depend on their respective concentrations and diffusion coefficients (see Eq. (6)), $\overline{C}$ and $\overline{D}$ are also shown in Fig. 7. For the counter-ion, the transport numbers calculated when Manning theory was included (red or blue lines) are lower than those calculated when Manning theory was not included (dashed black lines), as stated in the previous section. The counter-ion diffusion coefficients predicted by Manning theory are also lower than those predicted when Manning theory was not included (i.e., using the Mackie-Meares model), as shown in Fig. 7 (solid lines vs. dashed lines), illustrating that the lower value of $\bar{t}_{ct}$ predicted by Manning theory is caused by the lower diffusion coefficients, not differences in the ion activity.

The difference in diffusion coefficient values between the Manning and Mackie-Meares model scenarios is larger for the counter-ion than the co-ion because the Manning model assumes that counter-ions that are strongly paired with the fixed charged sites (i.e., condensed) have no mobility [54,57]. Thus, $f_{electric}$ in Eq. (28) has a different value for counter-ions and co-ions. This is an important and unique feature of the Manning model, and a contrast to the Mackie-Meares model we used for f_{steric}, which predicts the same reduction in mobility for both counter- and co-ions.

The prediction of the Manning diffusion model that the counter-ion is slowed to a greater degree than the co-ion also explains the asymmetric deviation potential results we observed for AEMs and CEMs in Fig. 5c. In bulk solution, Cl^- diffuses faster than Na^+. Therefore, in an AEM where Cl^- is the counter-ion, the Manning diffusion model tends to reduce the difference between the counter-ion and co-ion diffusion coefficients, while in a CEM where Na^+ is the counter-ion, it exaggerates the difference between them. This is evident in Fig. 7: for both AEMs, the numerical values of $\overline{D}_{ct}$ and $\overline{D}_{co}$ are similar, while for the CEMs, $\overline{D}_{ct}$ is roughly 50% of the value of $\overline{D}_{co}$. The prediction that co-ions diffuse faster in a CEM than counter-ions is inconsistent with recent experimental results by Kamcev et al. [57], and partly explains why including Manning theory in the model worsens the fit compared to the convection-only scenario. Ji et al. [9] recently showed that the ratio of counter-ion to co-ion diffusion coefficients inside an IEM has a strong effect on permselectivity; thus, errors in the relative magnitudes of $\overline{D}_{co}$ and $\overline{D}_{ct}$ would be expected to worsen the accuracy of model predictions. The authors of the Manning diffusion model have proposed an extension that improves its accuracy considerably by assigning different mobilities to condensed and uncondensed counter-ions [57], but we did not employ the extended model in this work because it introduces an additional adjustable parameter.

Continuing our comparison of transport numbers, we see in Fig. 7 that both the co-ion and water transport numbers are larger in the Manning scenario compared to the non-Manning model scenario. The larger counter-ion transport number in the non-Manning model scenario discussed above is compensated by smaller water and co-ion transport numbers, since the sum of transport numbers equals one by definition.

The shape of the transport number profiles is noteworthy. For all membranes, both $\bar{t}_{co}$ and $\bar{t}_{ct}$ decreased with distance from the high-concentration interface (increasing x), and were compensated by an increase in $\bar{t}_w$. The only variables that vary with x in Eqs. (6) and (7), which we used to calculate transport numbers, are $\overline{D}$ and $\overline{C}$. As Fig. 7 shows, the ion diffusion coefficients are essentially constant with position in the membrane. While this is expected in the non-Manning model scenario that uses the Mackie-Meares diffusion equation (Eq. (29)), the Manning theory diffusion equations (Eqs. (30) and (31)) depend on the local counter-ion concentration; however, Fig. 7 indicates that this dependence is weak. Because the diffusion coefficients within the membrane were nearly constant, changes in transport numbers within the membrane were caused by changes in concentration. For all membranes, counter- and co-ion concentrations were highest at the high-concentration interface and decreased towards the low-concentration interface. The decrease was especially pronounced for co-ions. Specifically, $\overline{C}_{co}$ was greater than 2 M at $x = 0$ but decreased below 0.02 M at $x = L$. Hence, the total migration flux carried by co-ions decreased with increasing x due to increasingly effective co-ion exclusion. Flux due to convection thus comprised a larger and larger fraction of total transport as x approached the dilute interface, as shown by the increasing value of $\bar{t}_w$ with x. The concentration profiles also illustrate that Donnan exclusion remains somewhat effective at $x = L$ even when it fails at $x = 0$ due to the high salt concentration. Hence, our modeling results provide an explanation for why apparent permselectivity is more sensitive to the low salt concentration than the high concentration.

6. Conclusion

In this work, we measured the apparent permselectivity of two anion and two cation exchange membranes when exposed to six different concentration gradients. We used a form of the extended Nernst-Planck equation to predict membrane potential and apparent permselectivity from measurable membrane characteristics such as charge concentration and water permeance. We examined the relative significance of convection, non-ideal ion behavior (i.e., activity and diffusion coefficients in the membrane), and the shape of the concentration profile in making accurate predictions of apparent permselectivity. The following points summarize our major findings:

- Modeling the membrane potential via the extended Nernst-Planck equation, which considers convection, coupled with ideal Donnan theory and the Mackie-Meares diffusion model enables accurate, quantitative predictions of membrane potential and apparent IEM permselectivity as a function of membrane properties and external salt concentrations. This model requires no adjustable parameters and only four measurements to characterize the IEM: water uptake, ion exchange capacity, water permeance, and thickness.
- Water transport through the IEM by osmosis plays a dominant role in reducing apparent permselectivity, even when the membrane is exposed to only moderate concentration differences (e.g. 0.5 M/0.1 M NaCl). Thus, including the effect of convection is essential for making accurate predictions of membrane permselectivity.
- Accounting for electrostatic effects in the ion activity and diffusion coefficients via Manning's counter-ion condensation theory resulted in less accurate predictions than assuming ideal behavior ($\Gamma = 1$) and considering only tortuosity (via the Mackie-Meares model). It appears that the lower accuracy of the model with Manning Theory is related to errors in the counter-ion diffusion coefficients predicted by the Manning model.
- The shape of the concentration profile appears to have little effect on model accuracy, implying that predicting the correct magnitude of

membrane interface quantities is much more important for the purposes of ion transport modeling than correct prediction of their profiles. This finding is mathematically expected when the transport numbers are relatively constant throughout the membrane.

- Apparent permselectivity is a strong function of the lowest salt concentration to which the membrane is exposed. As long as one salt concentration is relatively low (e.g., <0.1 M NaCl), reasonable permselectivity is maintained. We rationalize this finding with respect to our model results, which illustrate that Donnan exclusion at the low-concentration interface can remain effective even when it fails at the high-concentration interface.
- Strong osmotic deswelling benefits IEM permselectivity at high salt concentrations by increasing the fixed charge concentration and reducing the water permeability of the membrane. This suggests that non-reinforced or minimally-reinforced IEMs may give the best performance in applications involving very high salinities.

CRediT authorship contribution statement

R.S. Kingsbury: Methodology, Investigation, Software, Writing - original draft, Writing - review & editing, Conceptualization. **O. Coronell:** Writing - review & editing, Funding acquisition, Supervision, Conceptualization.

Declaration of competing interest

The authors declare that they have no known competing financial interests or personal relationships that could have appeared to influence the work reported in this paper.

Acknowledgement

This work was funded by the University of North Carolina Research Opportunities Initiative (ROI) program and the Gillings Innovation Labs Program of the University of North Carolina at Chapel Hill. R. Kingsbury was supported by the National Science Foundation Graduate Research Fellowship Program under Grant No. DGE-1144081. Any opinions, findings, and conclusions or recommendations expressed in this material are those of the authors and do not necessarily reflect the views of the National Science Foundation. The authors also thank Riley Vickers for assistance reviewing mathematical equations and model consistency.

Appendix A. Supplementary data

Supplementary data to this article can be found online at https://doi.org/10.1016/j.memsci.2020.118411.

References

[1] J. Kamcev, B.D. Freeman, Charged polymer membranes for environmental/energy applications, Annu. Rev. Chem. Biomol. Eng. 7 (2016) 111–133, https://doi.org/10.1146/annurev-chembioeng-080615-033533.
[2] Y. Mei, C.Y. Tang, Recent developments and future perspectives of reverse electrodialysis technology: a review, Desalination 425 (2017) 156–174, https://doi.org/10.1016/j.desal.2017.10.021.
[3] N.Y. Yip, D. Brogioli, H.V.M. Hamelers, K. Nijmeijer, Salinity gradients for sustainable energy: primer, progress, and prospects, Environ. Sci. Technol. 50 (2016) 12072–12094, https://doi.org/10.1021/acs.est.6b03448.
[4] A. Campione, L. Gurreri, M. Ciofalo, G. Micale, A. Tamburini, A. Cipollina, Electrodialysis for water desalination: a critical assessment of recent developments on process fundamentals, models and applications, Desalination 434 (2018) 121–160, https://doi.org/10.1016/j.desal.2017.12.044.
[5] G. Amy, N. Ghaffour, Z. Li, L. Francis, R.V. Linares, T. Missimer, S. Lattemann, Membrane-based seawater desalination: present and future prospects, Desalination 401 (2017) 16–21, https://doi.org/10.1016/j.desal.2016.10.002.
[6] A. Winger, G. Bodamer, R. Kunin, Some electrochemical properties of new synthetic ion exchange membranes, J. Electrochem. Soc. 100 (1953) 178–184.
[7] H. Fan, N.Y. Yip, Elucidating conductivity-permselectivity tradeoffs in electrodialysis and reverse electrodialysis by structure-property analysis of ion-exchange membranes, J. Membr. Sci. (2018), https://doi.org/10.1016/j.memsci.2018.11.045.
[8] A. Daniilidis, D.A. Vermaas, R. Herber, K. Nijmeijer, Experimentally obtainable energy from mixing river water , seawater or brines with reverse electrodialysis, Renew. Energy 64 (2014) 123–131, https://doi.org/10.1016/j.renene.2013.11.001.
[9] Y. Ji, H. Luo, G.M. Geise, Specific co-ion sorption and diffusion properties influence membrane permselectivity, J. Membr. Sci. 563 (2018) 492–504, https://doi.org/10.1016/j.memsci.2018.06.010.
[10] H.J. Cassady, E.C. Cimino, M. Kumar, M.A. Hickner, Specific ion effects on the permselectivity of sulfonated poly(ether sulfone) cation exchange membranes, J. Membr. Sci. 508 (2016) 146–152, https://doi.org/10.1016/j.memsci.2016.02.048.
[11] G.M. Geise, H.J. Cassady, D.R. Paul, E. Logan, M.A. Hickner, Specific ion effects on membrane potential and the permselectivity of ion exchange membranes, Phys. Chem. Chem. Phys. 16 (2014) 21673–21681, https://doi.org/10.1039/C4CP03076A.
[12] T. Luo, S. Abdu, M. Wessling, Selectivity of ion exchange membranes: a review, J. Membr. Sci. 555 (2018) 429–454, https://doi.org/10.1016/j.memsci.2018.03.051.
[13] N.Y. Yip, D.A. Vermaas, K. Nijmeijer, M. Elimelech, Thermodynamic, energy efficiency, and power density analysis of reverse electrodialysis power generation with natural salinity gradients, Environ. Sci. Technol. 48 (2014) 4925–4936, https://doi.org/10.1021/es5005413.
[14] C. Fernandez-Gonzalez, A. Dominguez-Ramos, R. Ibañez, Y. Chen, A. Irabien, Valorization of desalination brines by electrodialysis with bipolar membranes using nanocomposite anion exchange membranes, Desalination 406 (2017) 16–24, https://doi.org/10.1016/j.desal.2016.07.033.
[15] C. Fernandez-Gonzalez, A. Dominguez-Ramos, R. Ibañez, A. Irabien, Electrodialysis with bipolar membranes for valorization of brines, Separ. Purif. Rev. (2016), https://doi.org/10.1080/15422119.2015.1128951.
[16] C. Jiang, Y. Wang, Z. Zhang, T. Xu, Electrodialysis of concentrated brine from RO plant to produce coarse salt and freshwater, J. Membr. Sci. 450 (2014), https://doi.org/10.1016/j.memsci.2013.09.020.
[17] A. Emdadi, P. Gikas, M. Farazaki, Y. Emami, Salinity gradient energy potential at the hyper saline Urmia Lake – ZarrinehRud River system in Iran, Renew. Energy 86 (2016) 154–162, https://doi.org/10.1016/j.renene.2015.08.015.
[18] E. Farrell, M.I. Hassan, R.A. Tufa, A. Tuomiranta, A.H. Avci, A. Politano, E. Curcio, H.A. Arafat, Reverse electrodialysis powered greenhouse concept for water- and energy-self-sufficient agriculture, Appl. Energy 187 (2017) 390–409, https://doi.org/10.1016/j.apenergy.2016.11.069.
[19] M. Tedesco, A. Cipollina, A. Tamburini, G. Micale, J. Helsen, M. Papapetrou, REAPower: use of desalination brine for power production through reverse electrodialysis, Desalin. Water Treat. 53 (2014) 3161–3169, https://doi.org/10.1080/19443994.2014.934102.
[20] M. Tedesco, C. Scalici, D. Vaccari, A. Cipollina, A. Tamburini, G. Micale, Towards 1kW power production in a reverse electrodialysis pilot plant with saline waters and concentrated brines, J. Membr. Sci. 500 (2016) 33–45, https://doi.org/10.1016/j.memsci.2015.10.057.
[21] M. Tedesco, E. Brauns, A. Cipollina, G. Micale, P. Modica, G. Russo, J. Helsen, Reverse Electrodialysis with saline waters and concentrated brines: a laboratory investigation towards technology scale-up, J. Membr. Sci. 492 (2015) 9–20, https://doi.org/10.1016/j.memsci.2015.05.020.
[22] M. Bevacqua, A. Carubia, A. Cipollina, A. Tamburini, M. Tedesco, G. Micale, Performance of a RED system with ammonium hydrogen carbonate solutions, Desalin. Water Treat. 57 (2016) 23007–23018, https://doi.org/10.1080/19443994.2015.1126410.
[23] G.M. Geise, M.a. Hickner, B.E. Logan, Ammonium bicarbonate transport in anion exchange membranes for salinity gradient energy, ACS Macro Lett. 2 (2013) 814–817, https://doi.org/10.1021/mz4003408.
[24] X. Zhu, W. He, B.E. Logan, Influence of solution concentration and salt types on the performance of reverse electrodialysis cells, J. Membr. Sci. 494 (2015) 154–160, https://doi.org/10.1016/j.memsci.2015.07.053.
[25] W.J. van Egmond, M. Saakes, S. Porada, T. Meuwissen, C.J.N. Buisman, H.V.M. Hamelers, The concentration gradient flow battery as electricity storage system: technology potential and energy dissipation, J. Power Sources 325 (2016) 129–139, https://doi.org/10.1016/j.jpowsour.2016.05.130.
[26] W.J. van Egmond, U.K. Starke, M. Saakes, C.J.N. Buisman, H.V.M. Hamelers, Energy efficiency of a concentration gradient flow battery at elevated temperatures, J. Power Sources 340 (2017) 71–79, https://doi.org/10.1016/j.jpowsour.2016.11.043.
[27] R.S. Kingsbury, K. Chu, O. Coronell, Energy storage by reversible electrodialysis: the concentration battery, J. Membr. Sci. 495 (2015) 502–516, https://doi.org/10.1016/j.memsci.2015.06.050.
[28] M. Tedesco, A. Cipollina, A. Tamburini, I.D.L. Bogle, G. Micale, A simulation tool for analysis and design of reverse electrodialysis using concentrated brines, Chem. Eng. Res. Des. 93 (2015) 441–456, https://doi.org/10.1016/j.cherd.2014.05.009.
[29] A. Zlotorowicz, R.V. Strand, O.S. Burheim, Ø. Wilhelmsen, S. Kjelstrup, The permselectivity and water transference number of ion exchange membranes in reverse electrodialysis, J. Membr. Sci. (2016), https://doi.org/10.1016/j.memsci.2016.10.003.
[30] R.A. Tufa, E. Curcio, W. van Baak, J. Veerman, S. Grasman, E. Fontananova, G. Di Profio, Potential of brackish water and brine for energy generation by salinity gradient power-reverse electrodialysis (SGP-RE), RSC Adv. 4 (2014) 42617–42623, https://doi.org/10.1039/C4RA05968A.
[31] N.Y. Yip, M. Elimelech, Comparison of energy efficiency and power density in pressure retarded osmosis and reverse electrodialysis, Environ. Sci. Technol. 48 (2014) 11002–11012, https://doi.org/10.1021/es5029316.

[32] M. Tedesco, H.V.M. Hamelers, P.M. Biesheuvel, Nernst-Planck transport theory for (reverse) electrodialysis: I. Effect of co-ion transport through the membranes, J. Membr. Sci. 510 (2016) 370–381, https://doi.org/10.1016/j.memsci.2016.03.012.
[33] M. Tedesco, H.V.M. Hamelers, P.M. Biesheuvel, Nernst-Planck transport theory for (reverse) electrodialysis: II. Effect of water transport through ion-exchange membranes, J. Membr. Sci. 531 (2017) 172–182, https://doi.org/10.1016/j.memsci.2016.03.012.
[34] R.S. Kingsbury, S. Zhu, S. Flotron, O. Coronell, Microstructure determines water and salt permeation in commercial ion exchange membranes, ACS Appl. Mater. Interfaces 10 (2018) 39745–39756, https://doi.org/10.1021/acsami.8b14494.
[35] F. Helfferich, Ion Exchange, McGraw-Hill, New York, 1962.
[36] H. Strathmann, Introduction to Membrane Science and Technology, Wiley-VCH Verlag, Weinheim, Germany, 2011.
[37] T. Sata, Ion Exchange Membranes: Preparation, Characterization, Modification, and Application, Royal Society of Chemistry, Cambridge, 2004.
[38] H. Strathmann, Ion Exchange Membrane Separation Processes, Elsevier, Amsterdam, 2004.
[39] N.P. Berezina, N.A. Kononenko, O.A. Dyomina, N.P. Gnusin, Characterization of ion-exchange membrane materials: properties vs structure, Adv. Colloid Interface Sci. 139 (2008) 3–28, https://doi.org/10.1016/j.cis.2008.01.002.
[40] Y. Tanaka, Theory of teorell, meyer, and sievers (TMS theory), in: Ion Exch. Membr. Fundam. Appl., Elsevier, 2015, pp. 67–73, https://doi.org/10.1016/B978-0-444-63319-4.00003-1.
[41] J. Kamcev, D.R. Paul, B.D. Freeman, Ion activity coefficients in ion exchange polymers: applicability of Manning's counterion condensation theory, Macromolecules 48 (2015) 8011–8024, https://doi.org/10.1021/acs.macromol.5b01654.
[42] A.J. Bard, L.R. Faulkner, Electrochemical Methods: Fundamentals and Applications, second ed., John Wiley & Sons, 2001 https://doi.org/10.1016/j.aca.2010.06.020.
[43] J. Kamcev, M. Galizia, F.M. Benedetti, E.-S. Jang, D.R. Paul, B. Freeman, G. S. Manning, Partitioning of mobile ions between ion exchange polymers and aqueous salt solutions: importance of counter-ion condensation, Phys. Chem. Chem. Phys. (2016) 6021–6031, https://doi.org/10.1039/C5CP06747B.
[44] R.A. Robinson, R.H. Stokes, Electrolyte Solutions, Second Revised Edition, Butterworths, London, 1968.
[45] M. Galizia, G.S. Manning, D.R. Paul, B.D. Freeman, Ion partitioning between brines and ion exchange polymers, Polymer 165 (2019) 91–100, https://doi.org/10.1016/j.polymer.2019.01.026.
[46] H. Ohshima, S. Ohki, Donnan potential and surface potential of a charged membrane, Biophys. J. 47 (1985) 673–678, https://doi.org/10.1016/S0006-3495(85)83963-1.
[47] P.M. May, D. Rowland, G. Hefter, E. Königsberger, A generic and updatable pitzer characterization of aqueous binary electrolyte solutions at 1 bar and 25 °C, J. Chem. Eng. Data 56 (2011) 5066–5077, https://doi.org/10.1021/je2009329.
[48] K.S. Pitzer, G. Mayorga, Thermodynamics of electrolytes II. Activity and osmotic coefficients for strong electrolytes with one or both ions univalent, J. Phys. Chem. 77 (1973) 2300–2308.
[49] R. Schlögl, The significance of convection in transport processes across porous membranes, Discuss. Faraday Soc. 21 (1956) 46–52.
[50] A. Yaroshchuk, Current-induced concentration polarization of interfaces between non-ideally perm-selective ion-exchange media and electrolyte solutions, J. Membr. Sci. 396 (2012) 43–49, https://doi.org/10.1016/j.memsci.2011.12.029.
[51] M.W. Verbrugge, R.F. Hill, Ion and solvent transport in ion-exchange membranes. 1. A macrohomogeneous mathematical model, J. Electrochem. Soc. 137 (1990) 886–893, https://doi.org/10.1149/1.2086573.
[52] A.H. Galama, D.A. Vermaas, J. Veerman, M. Saakes, H.H.M. Rijnaarts, J.W. Post, K. Nijmeijer, Membrane resistance: the effect of salinity gradients over a cation exchange membrane, J. Membr. Sci. 467 (2014) 279–291, https://doi.org/10.1016/j.memsci.2014.05.046.
[53] P. Vanýsek, Ionic conductivity and diffusion at infinite dilution, in: W.M. Hamner (Ed.), CRC Handb. Chem. Phys., 92nd ed., 2011.
[54] J. Kamcev, D.R. Paul, G.S. Manning, B.D. Freeman, Predicting salt permeability coefficients in highly swollen, highly charged ion exchange membranes, ACS Appl. Mater. Interfaces 9 (2017) 4044–4056, https://doi.org/10.1021/acsami.6b14902.
[55] J.S. Mackie, P. Meares, The diffusion of electrolytes in a cation-exchange resin membrane. I. Theoretical, Proc. Roy. Soc. Lond. A. 232 (1955) 498–509.
[56] J.S. Mackie, P. Meares, The diffusion of electrolytes in a cation-exchange resin membrane. II. Experimental, Proc. Roy. Soc. Lond. A. 232 (1955) 510–518.
[57] Jovan Kamcev, Donald R. Paul, Gerald S. Manning, Benny D. Freeman, Ion diffusion coefficients in ion exchange membranes: significance of counter-ion condensation, Macromolecules (2018), https://doi.org/10.1021/acs.macromol.8b00645.
[58] R.S. Kingsbury, K. Bruning, S. Zhu, S. Flotron, C.T. Miller, O. Coronell, Influence of water uptake, charge, Manning parameter and contact angle on water and salt transport in commercial ion exchange membranes, Ind. Eng. Chem. Res. 58 (2019) 18663–18674, https://doi.org/10.1021/acs.iecr.9b04113.
[59] G.M. Geise, D.R. Paul, B.D. Freeman, Fundamental water and salt transport properties of polymeric materials, Prog. Polym. Sci. 39 (2014) 1–42, https://doi.org/10.1016/j.progpolymsci.2013.07.001.
[60] R.S. Kingsbury, S. Flotron, S. Zhu, D.F. Call, O. Coronell, Junction potentials bias measurements of ion exchange membrane permselectivity, Environ. Sci. Technol. 52 (2018) 4929–4936, https://doi.org/10.1021/acs.est.7b05317.
[61] K.J. Irwin, S.M. Barnett, D.L. Freeman, Quantum mechanical studies of local water structure near fixed ions in ion exchange membranes, J. Membr. Sci. 47 (1989) 79–89, https://doi.org/10.1016/S0376-7388(00)80861-3.
[62] H.B. de Aguiar, D. Ben-Amotz, S. Roke, Y. Chen, B.M. Rankin, R. Scheu, Specific ion effects in amphiphile hydration and interface stabilization, J. Am. Chem. Soc. 136 (2014) 2040–2047, https://doi.org/10.1021/ja4120117.
[63] E. Güler, R. Elizen, D.A. Vermaas, M. Saakes, K. Nijmeijer, Performance-determining membrane properties in reverse electrodialysis, J. Membr. Sci. 446 (2013) 266–276, https://doi.org/10.1016/j.memsci.2013.06.045.